Supporting Information

Thermal Switching of Brønsted Acid Sites in Defective UiO-66 Governs the Activity of Fructose Dehydration to 5-Hydroxymethylfurfural

Kai Yan,[a] Zhihao Yu,[a,b]* Yingqing Li,[a] Mengyan Guo,[a] Yuanyu Wang,[a] Xuebin Lu[a,c]*

a. School of Environmental Science and Engineering, Tianjin University, Tianjin 300350, P. R. China
b. Institute for Catalysis, Hokkaido University, Sapporo, 001–0021, Japan
c. School of Ecology and Environment, Xizang University, Lhasa 850000, P. R. China

E-mail: zhihaoyupublic@tju.edu.cn, xbltju@tju.edu.cn

1. Experimental

1.1 Characterization

Scanning electron microscopy (SEM, S-4800, HITACHI) was employed to examine the morphology and particle size of the catalysts. Powder X-ray diffraction (PXRD) patterns were recorded on a Bruker D8 X-ray diffractometer using Cu Kα radiation (40 kV, 40 mA). X-ray photoelectron spectroscopy (XPS) was performed on a Thermo Escalab 250XI spectrometer (USA) with Al Kα radiation as the X-ray source. The binding energies of Zr 3d were calibrated with reference to the C 1s spectral line at 284.8 eV. The Brunauer–Emmett–Teller (BET) specific surface area was determined using an ASAP 2460 instrument (Micromeritics) at -196 °C via N_2 adsorption-desorption isotherms. All samples were degassed under a N_2 stream at 180 °C for 8 h prior to measurement. Thermogravimetric analysis (TGA) was performed on a NETZSCH STA 449 F3 instrument using alumina crucibles. Samples were weighed before testing and heated from room temperature to 800 °C at a rate of 10 °C min^{-1}. FT-IR spectra were recorded using a FOLI10-R Fourier transform infrared spectrometer (Yingsa Optics, Shanghai) equipped with an MCT detector (32 scans, 4 cm^{-1} resolution). Background spectra were recorded under vacuum degassing and subtracted from the sample spectra. The FT-IR was conducted using pyridine and CD_3CN as probe molecules.

1.2 Reaction Evaluation

The dehydration of fructose was performed in a 25 mL stainless-steel high-pressure reactor equipped with temperature and pressure control and a magnetic stirrer. Typically, the reactor was charged with fructose (50 mg), catalyst (20 mg), and solvent (5 mL). The reaction was conducted at different temperatures under stirring at 800 rpm. After completion, the reactor was cooled using an ice-water bath, and the suspension was filtered to separate the catalyst and collect the liquid products.

All liquid products were analyzed by high-performance liquid chromatography (HPLC) using a Bio-Rad Aminex HPX-87H column (300 mm × 7.8 mm). The mobile phase was 4 mM H_2SO_4, the flow rate was 0.45 mL min^{-1}, and the column temperature was maintained at 60 °C.

Fructose conversion and HMF yield were determined by the following equations:

$$\text{Frutose conversion } (\%) = \frac{\text{Mole of converted frutose}}{\text{Mole of initial frutose}} \times 100\% \quad (1)$$

$$\text{HMF yield } (\%) = \frac{\text{Mole of produced HMF}}{\text{Theoretically maximum mole of HMF}} \times 100\% \quad (2)$$

1.3 Catalyst Recycling

The recyclability of the catalyst was evaluated under identical reaction conditions. After each catalytic run, the solid catalyst was recovered by filtration, thoroughly washed, and dried at 200 °C under vacuum. The regenerated catalyst was subsequently reused directly in the next reaction cycle without any further treatment. Fructose conversion and HMF yield were monitored after each cycle to assess the catalytic stability and reusability of the catalyst over multiple runs.

2. Supporting Figures and Tables

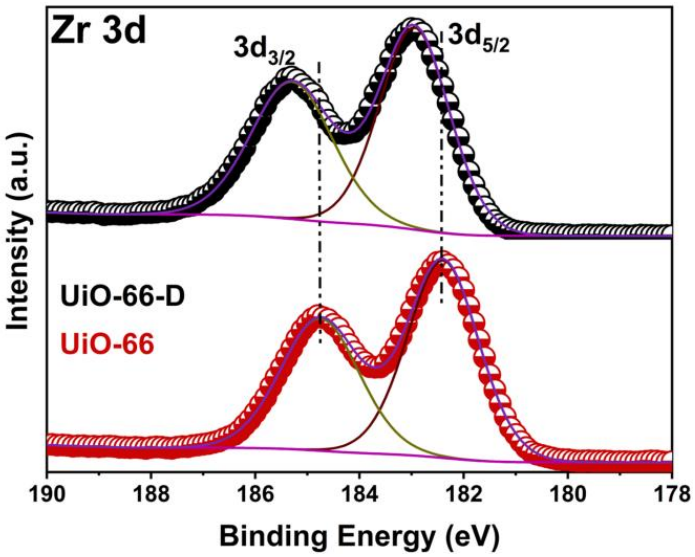

Figure S1. High-resolution XPS spectra (Zr 3d) of UiO-66 and UiO-66-D.

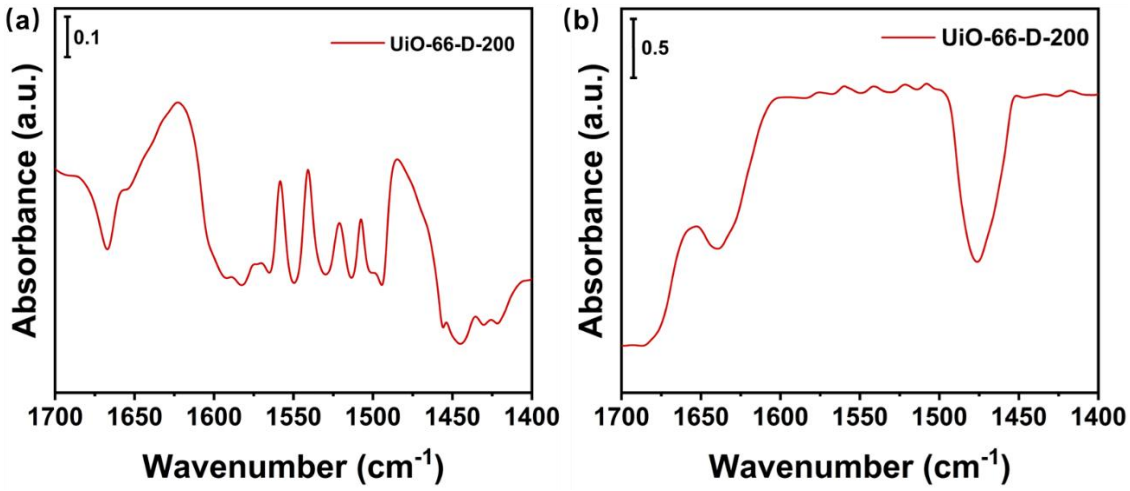

Figure S2. (a) Difference FT-IR spectrum of pyridine-absorbed UiO-66-D-200. (b) FT-IR spectrum of UiO-66-D-200.

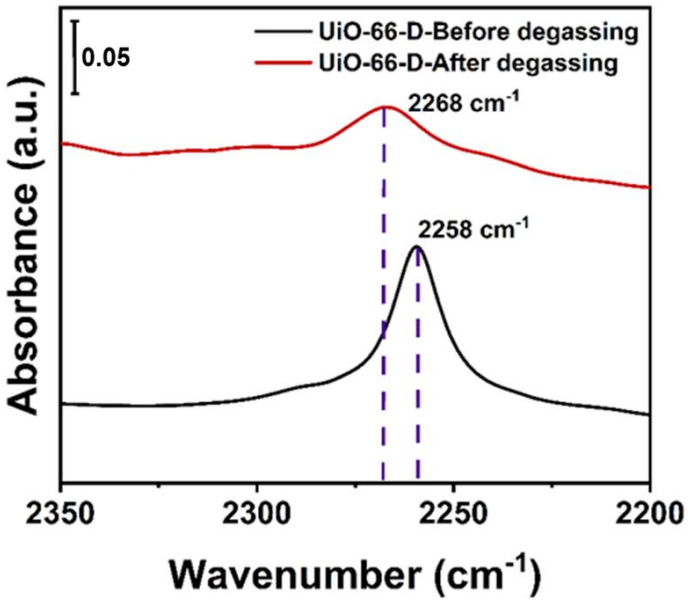

Figure S3. Difference FT-IR spectra of CD_3CN-adsorbed UiO-66-D.

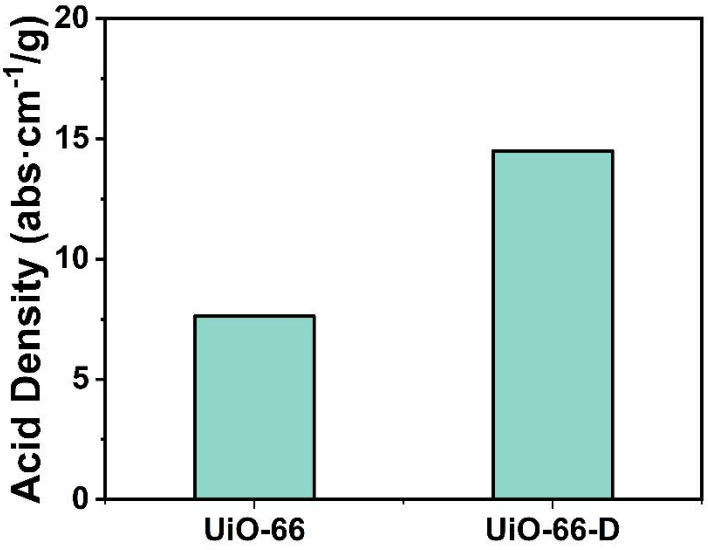

Figure S4. Acid density of UiO-66 and UiO-66-D. Acid density is calculated using the absorption peak area as a substitute indicator due to the absence of the extinction coefficient in current literature.

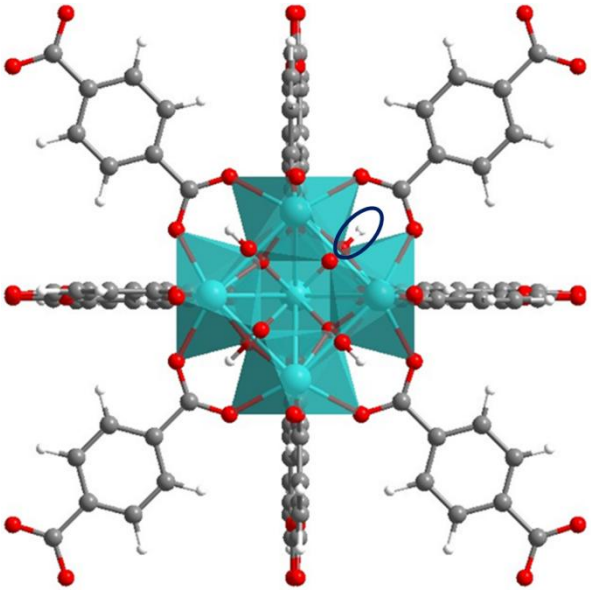

Figure S5. View of μ_3−OH in one metal cluster. Zr = cyan spheres, O = red spheres, C = gray spheres, H = white spheres.

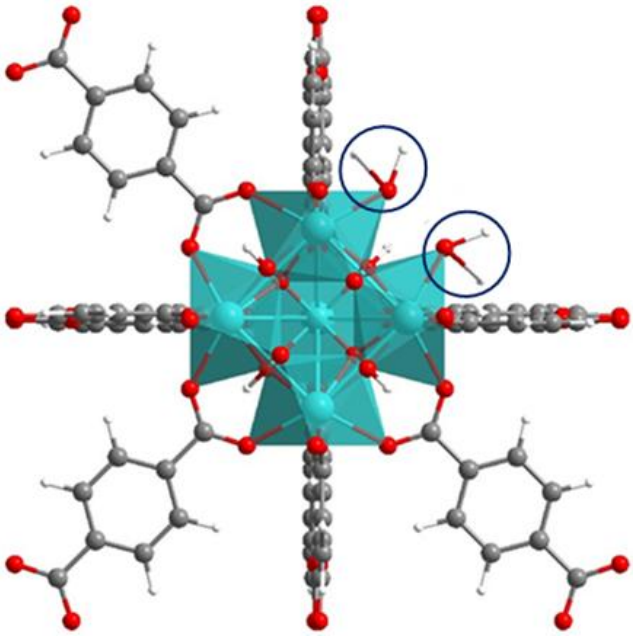

Figure S6. View of Zr−H_2O in one metal cluster with a defect site where TPA is replaced by water. Zr = cyan spheres, O = red spheres, C = gray spheres, H = white spheres.

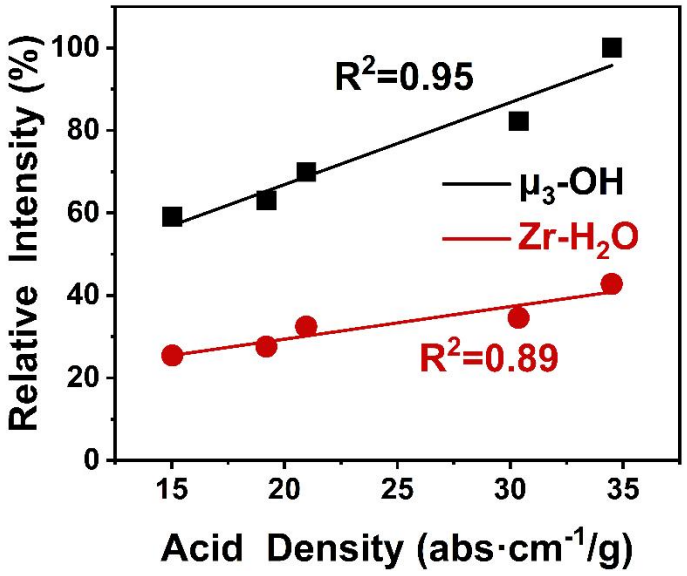

Figure S7. Linear fitting relationship between acid density and relative intensity of Zr-H_2O and μ_3−OH.

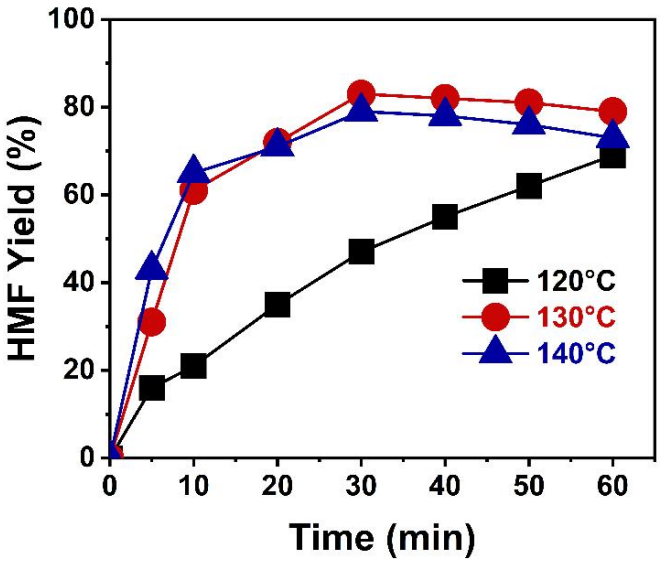

Figure S8. Effects of temperature on the reaction activity of fructose dehydration by using UiO-66-D-200. Reaction conditions: 50 mg fructose, 5 mL DMSO, 20 mg catalyst

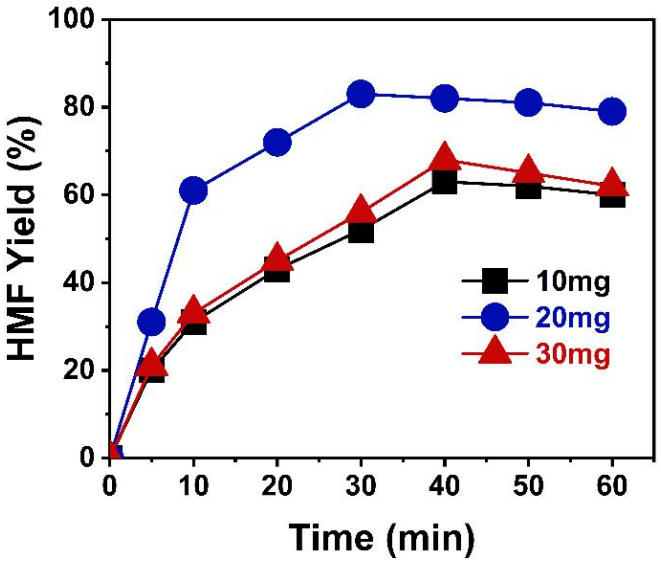

Figure S9. Effects of catalyst dosage on the activity of fructose dehydration by using UiO-66-D-200. Reaction conditions: 50 mg fructose, 5 mL DMSO, 130 °C.

Table S1. Physicochemical properties of UiO-66 and UiO-66-D.

Catalyst	S_{BET} ($m^2 g^{-1}$)	Total pore volume ($cm^3 g^{-1}$)	Average pore size (nm)
UiO-66	287.8	0.1	1.9
UiO-66-D	238.7	0.2	2.1

Table S2. Comparison of the reaction performance of UiO-66-D-200 with previously reported MOF-based catalysts.

Entry	Catalyst	Fructose amount (mg)	Solvent	Temperature (°C)	Time (min)	Yield (%)	Ref.
1	Pd NPs/Sn-Na MOF	10	Water	140	180	73.1	1
2	UiO-66-NH_2	25	DMSO	120	60	43.0	2
3	MIL-101	500	DMSO	120	60	63.0	3
4	MIL-101	250	DMSO	120	120	39.5	4
5	T-CeMOF[1]	200	H_2O/EtOH	160	60	67.2	5
6	MOF-PMAi-Br[2]	500	DMSO	100	60	42.0	6
7	ADES-4[3]	10	DMSO	120	60	75.0	7
8	ADES-5[4]	10	DMSO	120	60	73.9	7
9	UiO-66-D-200	50	DMSO	130	30	83.0	This work

Notes: [1] Taurine-involved Ce-based MOF (T-CeMOF), [2] Brominated polymer composite material (MOF-PMAi-Br), [3-4] Functional neutral metal–organic frameworks (MOFs) {[M(5OH-IP)(L)]}.$_n$ [M = Zn(II) for ADES-4; Cd(II) for ADES-5.

References

1. J. Rohilla, S. Thakur, K. Kumar, R. Singh and V. Kaur, ACS Appl. Nano Mater., 2023, 6, 12063-12072, DOI: 10.1021/acsanm.3c01842.
2. Y. Zhong, C. Huang, L. Li, Q. Deng, J. Wang, Z. Zeng and S. Deng, Chinese J. Chem. Eng., 2022, 49, 245-252, DOI: 10.1016/j.cjche.2021.08.004.
3. H. Li, Y. Zhong, L. Wang, Q. Deng, J. Wang, Z. Zeng, X. Cao and S. Deng, Chinese J. Chem. Eng., 2021, 33, 167-174, DOI: 10.1016/j.cjche.2020.09.018.
4. Y. Zhong, Q. Yao, P. Zhang, H. Li, Q. Deng, J. Wang, Z. Zeng and S. Deng, Ind. Eng. Chem. Res., 2020, 59, 22068-22078, DOI: 10.1021/acs.iecr.0c04798.
5. C. Wang, K. Li and P. Ji, J. Chem. Technol. Biotechnol., 2021, 96, 163-171, DOI: 10.1002/jctb.6522.
6. L. Bromberg, X. Su and T. A. Hatton, Chem. Mater., 2014, 26, 6257-6264, DOI: 10.1021/cm503098p.
7. U. Patel, B. Parmar, A. Dadhania and E. Suresh, Inorg. Chem., 2021, 60, 9181-9191, DOI: 10.1021/acs.inorgchem.1c01208.